Bias corrections for speciated and source-resolved $PM_{2.5}$ chemical transport model simulations using a geographically weighted regression

Carlos S. Hernandez[1], Ksakousti Skyllakou[2], Pablo Garcia Rivera[3], Brian Dinkelacker[3], Julian D. Marshall[4], C. Arden Pope III[5], Allen L. Robinson[6], Spyros N. Pandis[2,7], and Peter J. Adams[1,8,*]

[1] Department of Civil and Environmental Engineering, Carnegie Mellon University, Pittsburgh, PA, USA
[2] Institute of Chemical Engineering Sciences (FORTH/ICE-HT), Patras, Greece
[3] Department of Chemical Engineering, Carnegie Mellon University, Pittsburgh, PA, USA
[4] Department of Civil and Environmental Engineering, University of Washington, Seattle, WA, USA
[5] Department of Economics, Brigham Young University, Provo, UT, USA
[6] Department of Mechanical Engineering, Carnegie Mellon University, Pittsburgh, PA, USA
[7] Department of Chemical Engineering, University of Patras, Greece
[8] Department of Engineering and Public Policy, Carnegie Mellon University, Pittsburgh, PA, USA

* Corresponding author: peteradams@cmu.edu

Abstract: The ability to provide speciated and source-resolved $PM_{2.5}$ estimates make chemical transport models a potentially valuable tool for exposure assessments. However, epidemiological studies often require unbiased estimates, which can be challenging for chemical transport models. We use geographically weighted regression to predict and correct the bias in source-resolved $PM_{2.5}$ species (elemental carbon, organic aerosol, ammonium, nitrate, and sulfate) across the continental U.S. for 2001 and 2010. The regression models are trained using speciated ground-level monitors from the CSN and IMPROVE networks. A 10-fold cross-validation shows minimal bias across all simulated $PM_{2.5}$ species (0 – 3%) and improved agreement with ground-level monitors (R^2 = 0.53 – 0.97). Corrections also improve the agreement between simulated and observed species mixtures on a fractional basis. The source-resolved exposure estimates developed in this study are suitable for use in health analyses of $PM_{2.5}$ toxicity.

Introduction

Chronic exposure to fine particulate matter ($PM_{2.5}$) is known to lead to negative human health outcomes (Pope et al., 2020; Pope and Dockery 2006) and is the leading contributor to morbidity and mortality among air pollutants (Lefler et al., 2019; Cohen et al., 2017). Air quality management in the United States has effectively reduced concentrations of $PM_{2.5}$ (Zhang et al., 2018), with health benefits consistently exceeding the cost of regulations (U.S. EPA, 2012, 2011, 1999). Several studies suggest that further reductions of $PM_{2.5}$ in the U.S. would lead to increased life expectancy (Bennet et al., 2019; Apte et al., 2018; Correia et al., 2013; Pope et al., 2009). To date, air quality regulations have targeted $PM_{2.5}$ by total mass, with the implicit assumption that all $PM_{2.5}$ is equally toxic. However, $PM_{2.5}$ is a complex mixture with varying properties, including but not limited to size, phase, acidity, chemical composition and source. Given the various pathophysiological pathways for $PM_{2.5}$-induced morbidity and mortality (Pope and Dockery, 2006), it is plausible for $PM_{2.5}$ toxicity to be a function of its properties. Identifying more toxic components could lead to more effective regulations. However, prior work has been unable to conclusively identify the key drivers of $PM_{2.5}$ toxicity (Kelly and Fussell, 2012; Harrison and Yin, 2000). To investigate this question further in epidemiological studies, accurate exposure estimates of $PM_{2.5}$ and its properties are necessary.

Conventional $PM_{2.5}$ exposure estimates for health studies are primarily derived from observations. Data from ground-level monitors and satellites are used with empirical models to provide accurate and consistent assignment of $PM_{2.5}$ exposures in epidemiological studies. Additionally, land use variables and meteorological data, which can provide additional information on the spatiotemporal variability of $PM_{2.5}$, have been successfully used in empirical models to enhance the accuracy, resolution and extent of exposure estimates. Because of their dependence on observations, empirical estimates can be sensitive to data availability and by definition lack a mechanistic basis. The latter can make it difficult for empirical models to estimate $PM_{2.5}$ species, sources, and other properties with limited data.

Alternatively, chemical transport models (CTMs) readily predict a wide range of $PM_{2.5}$ characteristics and properties, such as chemical composition and source, that are often limited in observational datasets. Despite this, CTMs alone are unable to match the accuracy and consistency of empirical estimates. Known biases resulting from errors in emission inventories, chemical mechanisms, coarse grid resolution, large emissions gradients, complex terrain and meteorology make unprocessed CTM estimates unreliable for epidemiological analyses. The underlying causes of CTM biases can also change with space, resulting in different regions having characteristic biases and errors. A statistical technique that can identify and remediate regionally varying biases in CTM estimates could facilitate their use in epidemiological analyses, and provide much needed information on $PM_{2.5}$ properties.

Geographically weighted regression (GWR) is a local spatial analysis technique that models the spatially-varying relationships between independent and dependent variables (Brunsdon et al., 1996). Regression coefficients in GWR are determined locally, which could allow for targeted identification of regional biases in simulated $PM_{2.5}$. Several studies have used GWR to develop $PM_{2.5}$ exposure estimates, primarily as a predictive tool to correct satellite AOD measurement to ground-level monitors (Hammer et al., 2020; van Donkelaar et al., 2019, 2016, 2015; Meng et al., 2019; Zhai et al., 2018; Li et al., 2017a; You et al., 2016; Song et al., 2014; Ma et al., 2014; Hu et al., 2013; Hu, 2009). A subset of these studies has also incorporated information from CTMs, like spatiotemporal extent of $PM_{2.5}$ (Hammer et al., 2020; van Donkelaar et al., 2019, 2016, 2015; Meng et al., 2019; Li et al., 2017a). However, only one uses CTMs to predict the chemical composition of $PM_{2.5}$ (van Donkelaar et al., 2019). In the broader literature, studies using techniques other than GWR have also incorporated CTMs in exposure estimates (Huang et al., 2021; Berrocal et al., 2020; Lyu et al., 2019; Geng et al., 2017, 2015; Wang et al., 2016; Lee et al., 2012). However, most of these studies used CTMs to inform the spatiotemporal extent of total $PM_{2.5}$ mass, while only a few used information on chemical composition (Li et al., 2017b; Geng et al., 2017; Philip et al., 2014). To our knowledge, no study has generated exposure estimates that resolve multiple properties of $PM_{2.5}$ across the entire continental U.S.

In this work, we use GWR to correct biases in speciated and source-resolved CTM simulations. These estimates are developed by integrating CTM simulations, observations from speciated ground-level monitors, geographic variables and other empirical estimates. Briefly, PMCAMx is used to simulate $PM_{2.5}$ over the continental U.S. for 2001 and 2010 using a methodologically consistent emissions inventory. The Particulate Source Apportionment Technology (PSAT) algorithm is used to tag 6 source categories which include EGU, non-EGU, on-road, non-road, biogenic and other emissions. Annually averaged simulations are corrected to speciated ground-level monitors by using GWR to predict the bias in simulated $PM_{2.5}$ species, similar to work conducted in van Donkelaar et al. (2019). Geographic variables, empirical estimates and CTM estimates are used as predictors in the GWR model. Species corrected in this study include elemental carbon (EC), organic aerosol (OA), ammonium (NH_4^+), nitrate (NO_3^-) and sulfate (SO_4^{2-}). Original source mixtures as predicted by the CTM are preserved and applied proportionally to the corrected estimates. Species- and source-resolved $PM_{2.5}$ exposure estimates described in this work are freely and publicly available at www.caces.us.

Methods

PMCAMx Chemical Transport Model

A brief description of the underlying CTM simulations follows, but they are more fully described in Skyllakou et al. (in review). We use the PMCAMx model (Karydis et al., 2010; Murphy and Pandis, 2010; Tsimpidi et al., 2010; Posner et al., 2019) with a "source tagging" algorithm, PSAT (Wagstrom et al., 2008; Wagstrom and Pandis, 2011a, 2011b; Skyllakou et al., 2014, 2017), that facilitates tracking source apportionment in a computationally efficient way. The model domain covers the continental U.S., portions of Canada and Mexico, and nearby offshore regions at a horizontal resolution of 36 km. We perform simulations for the years 1990, 2001, and 2010 using a methodologically consistent set of emission inventories (Xing et al., 2013). Several broad source categories are resolved for this analysis. The EGU category includes emissions from electricity-generating units included in EPA's Integrated Planning Model. Non-EGU includes other industrial point sources. The on-road category includes mobile emissions from roads in the continental U.S., while the non-road category includes all off-road mobile emissions in the model domain. Biogenic includes emissions from vegetation. The "other" category includes on-road vehicles from Canada and Mexico plus all other emissions. Emissions from the model's boundary and initial conditions are also tracked as separate categories. Species predicted by the model and used in this work include SO_4^{2-}, NO_3^-, $NH4^+$, EC, primary organic aerosol (POA) and secondary organic aerosol (SOA). PMCAMx uses an advanced treatment of OA that accounts for the semi-volatile nature of primary organic emissions and recent advances in our understanding of SOA chemistry (Murphy and Pandis, 2009; Robinson et al., 2007, Donahue et al., 2006). The model also predicts concentrations of sodium, chloride, and mineral dust, but these are excluded from this analysis due to large uncertainty in the emissions inventory and because speciated monitors for these species are not readily available. Meteorological data input to PMCAMx are taken from simulations performed with the Weather Research Forecasting model (WRF v3.6.1) for these time periods with boundary conditions from the ERA-Interim global climate re-analysis database.

Ground-level Speciated $PM_{2.5}$ Observations

Observations of $PM_{2.5}$ species (EC, OC, NH_4^+, NO_3^-, SO_4^{2-}) were obtained from the EPA Chemical Speciation Network (CSN) and the IMPROVE monitoring network for 2001 and 2010. Measurements were downloaded from the Federal Land Manager Environmental Database (http://views.cira.colostate.edu/fed/). Prior to the CSN transition period from 2007-2009, CSN and IMPROVE used different analytical and sampling protocols for carbon measurements, requiring harmonization across the datasets (Spada and Hyslop, 2018; Solomon et al., 2014; Malm et al., 2011). Most notably, pre-transition CSN monitors used the thermal optical transmittance (TOT) analytical protocol for carbon measurements, while IMPROVE and post-transition CSN monitors use the thermal optical reflectance (TOR) protocol. We adjust 2001 CSN carbon measurements to match post-transition CSN protocols following the approach in Lordo et al. (2016). Additionally, a filter blank correction of 0.4 μg m^{-3} is applied to organic carbon (OC) measurements in 2010. To account for differences in aging of organic aerosol in urban and rural areas, an OC:OA ratio of 1.4 and 1.8 was applied to OC measurements collected at CSN and IMPROVE sites, respectively. The number of speciated monitors used in the observational dataset is shown in Table 1. On average, 23 CSN and 92 IMPROVE monitors were used in 2001, while 165 CSN and 146 IMPROVE monitors were used in 2010. The increase in speciated monitors from 2001 to 2010 is notable, particularly in the eastern U.S., and its effects on model training are discussed in the results section.

Geographically Weighted Regression

In this study, GWR is used as a spatial extension of ordinary least squares (OLS) regression. Observations are weighted in the regression according to their proximity to a desired prediction point in space. A consequence of this formulation is that there is no global model (i.e., no global regression coefficients, which instead vary in space). Instead, the model is solved locally for every prediction point in space such that:

$$X^T W(i) X \beta(i) = X^T W(i) Y \ (eqn. 1)$$

where X is a matrix containing predictor variables, W is a weighting matrix (kernel) at location i, β is a vector of regression coefficients at location i, and Y is the dependent variable. The weighting matrix is a diagonal matrix, where each diagonal element is the weight assigned to an observation and is calculated by a user-defined weighting function (eqn. 2). Selection of the weighting function depends largely on the nature of the dataset. Weighting functions are typically calibrated to an optimal bandwidth, which controls the rate observations are down-weighted with distance. Weighting functions can also have cut-offs, which exclude observations past a certain threshold. Common weighting functions include inverse distance weighting and a Gaussian function. The results presented in this paper use a Gaussian weighting function:

$$w_{ij} = \exp\left(-\alpha d_{ij}^2\right) \ (eqn. 2)$$

where w_{ij} is the weight assigned to an observation in location j for predictions in location i, α is the decay coefficient or bandwidth, and d is the distance between location i and j. The bandwidth (α) is calibrated by minimizing the root mean square error in the GWR model. With eqn. 2, a bandwidth of zero leads to equal weighting for all observations, making the GWR model equivalent to OLS.

GWR is used to predict the bias in simulated $PM_{2.5}$ species, with GWR models being trained for each species and simulation year. Bias predictions are made at the centroids of U.S. census tracts and used to correct CTM simulations projected to census tracts. The GWR model form is:

$$(sim\,SPEC\ - obs\,SPEC) = \beta_{ED}ED + \beta_{IDU}IDU + \beta_{IEGb}IEGb + \sum \beta_c\, sim\,SPEC_c \quad (eqn.\,3)$$

The left-hand side of eqn. 3 represents the CTM bias relative to speciated ground-level monitors (i.e., outcome variable), while the right-hand side contains predictor variables. *SPEC* represents $PM_{2.5}$ species (e.g., EC, OA, NH_4^+, NO_3^-, SO_4^{2-}). *ED* represents the sub-grid elevation difference, which is the difference between the elevation of a prediction point and the mean elevation of the overlying CTM grid cell. Elevation is determined by the NOAA ETOP1 global relief model (NOAA, 2009; Amante and Eakins, 2009). *ED* is used as a measure of sub-grid terrain complexity that may contribute to model error. *IDU* is the inverse distance to the nearest urban land cover as determined by using year-specific MODIS MCD12Q1 land cover data (Friedl and Sulla-Menashe, 2019). Higher spatial variability is expected in urban areas, potentially contributing to model error at a relatively coarse horizontal resolution of 36 km. A maximum limit of 2 km^{-1} is set for *IDU* to avoid arbitrary variations above that threshold. *IEGb* is the total $PM_{2.5}$ bias of the CTM relative to predictions of the Integrated Empirical Geographic (IEG) model from Kim et al. (2020). The IEG model estimates annual averages of total $PM_{2.5}$ using ground-level monitor data, universal kriging and partial least squares of geographic variables which include land use variables and satellite estimates. *IEGb* serves as a useful initial guess of the bias, especially in regions where monitors are sparse. The final predictor variables, $SPEC_c$, are a subset of simulated species from the CTM. When predicting the bias of carbonaceous species, $SPEC_c$ represents the subset of all carbonaceous species (EC, POA, SOA). Likewise, when predicting the bias of a non-carbonaceous species, $SPEC_c$ represents the subset of all non-carbonaceous species (NH_4^+, NO_3^-, SO_4^{2-}). This is meant to limit the number of predictor variables in the model. While the CTM provides predictions of POA and SOA, there is not enough information on the aged nature of measured OC in order to model biases in POA and SOA directly. Instead, GWR is trained to model biases in total OA, and simulated POA and SOA are used as separate independent variables when applicable. After total OA is corrected, primary and secondary fractions as predicted by the CTM are applied proportionally to corrected OA. While corrected estimates of OA, POA and SOA are made available, only those for total OA are fully evaluated in this study.

Predicting CTM biases at a census tract resolution accomplishes several objectives. Predicted biases can be used to downscale CTM estimates with relatively coarse horizontal resolution. Additionally, it efficiently targets urban and population-dense areas, where $PM_{2.5}$ experiences greater spatial variability, for higher resolution corrections. Conversely, rural and low populations areas are given lower resolution corrections. Finally, it facilitates population-weighted averaging to coarser census geographies, such as counties or metropolitan statistical areas (MSAs). This allows epidemiological analyses to be easily performed at the desired resolution.

GWR models are evaluated using three cross-validation methods: 1) leave-one-out 2) 10-fold and 3) a regional holdout cross-validation (CV). The regional holdout CV functions similarly to the leave-one-out CV except that all monitors within a 400 km radius are excluded from model training. Because ground-level monitors tend to be spatially clustered, as opposed to randomly distributed, evaluations from a 10-fold CV may be less robust where monitors are absent. The regional holdout CV is designed to address this gap by rigorously testing model performance in areas with low monitor density. Model training, prediction and evaluation are performed on the R open-source software with community-developed packages (R Core Team 2021).

Results & Discussion

CTM & GWR Evaluation

We compared estimates of total uncorrected $PM_{2.5}$ from the CTM to those from the IEG model (Kim et al., 2020) and found significant regional biases in the raw CTM predictions. Spatially inconsistent biases are problematic for epidemiological studies because differences in $PM_{2.5}$ exposures cannot be adequately attributed to differences in health responses. This underscores the importance of correcting biases in CTM estimates with the GWR model.

Figure 1 shows the population-weighted bias between CTM and IEG model estimates at the county level. The leftmost panel illustrates the bias in uncorrected total $PM_{2.5}$ as estimated by the CTM. In the eastern U.S., CTM estimates are generally overestimated by 2 to 4 $\mu g\ m^{-3}$ when compared to the IEG model. In the western U.S., CTM estimates are generally underestimated when compared to the IEG model, with biases ranging from 0.1 to -1.6 $\mu g\ m^{-3}$. The middle panel in Figure 1 illustrates the bias when crustal PM and sea salt are removed from CTM estimates. Removing crustal PM and sea salt decreases the bias by 4 to 7 $\mu g\ m^{-3}$ in the eastern U.S., and by approximately 1 $\mu g\ m^{-3}$ in the western U.S. This suggests that crustal PM and seal salt could be responsible for the CTM's initial overprediction in the eastern U.S. Previous studies have noted large uncertainties associated with crustal PM in emission inventories (Xu et al., 2019, Appel et al., 2013), making their predicted source mixtures potentially unreliable. However, different regional biases persist after removing crustal PM and sea salt. On average, biases in the western U.S. are 0.8 $\mu g\ m^{-3}$ lower than in the eastern U.S. In California, where CTM underpredictions are most severe, biases are typically 2.9 and 3.7 μg m^{-3} lower than in the eastern U.S. for 2001 and 2010, respectively.

GWR corrections address spatial inconsistencies in total $PM_{2.5}$ bias and improve the performance of all species across several evaluation metrics. Model evaluations for uncorrected and GWR-corrected $PM_{2.5}$ species are shown in Figure 2 a) and b) for simulation years 2001 and 2010, respectively. Results from the 10-fold CV are shown for GWR-corrected species in Figure 2. Uncorrected OA and NO_3^- tend to be severely underpredicted in the west, often by a factor of 2 or more. Meanwhile, OA in the east tends to be slightly overpredicted, particularly in the southeast. GWR corrections improve R^2 coefficients for simulated OA and NO_3^- from 0.30 – 0.50 to 0.53 – 0.87. While overall error and bias are improved for OA and NO_3^-, some error persists for western corrections, particularly for OA. This could reflect a need to find predictor variables that better explain the bias for OA and NO_3^- in the western U.S. For $NH_4^+$and SO_4^{2-}, GWR corrections improve upon the already good performance of the original CTM results. In the west, NH_4^+ tends to be underpredicted, while SO_4^{2-} is slightly overpredicted. GWR addresses both biases and improves R^2 coefficients from 0.70 - 0.97 to 0.84 - 0.97. Successfully modeling EC is challenging due to its highly variable nature and the CTM's coarse resolution. However, GWR corrections do make significant improvements to simulated EC. Uncorrected EC simulations tend to be noisy and correlate poorly with monitors, with R^2 coefficients of 0.38 and 0.52 in 2001 and 2010, respectively. GWR corrections significantly reduce error and bias and increase R^2 coefficients to 0.62 and 0.71 in 2001 and 2010, respectively. Despite geographic differences in the biases, GWR models successfully improve model performance in regionally specific ways.

GWR corrections are largely robust across the three cross-validation methods used. In Figure 3, uncorrected and corrected simulated species are evaluated against observations by summarizing fractional bias, fractional error, and R^2 coefficients. All three CV results show significant reductions in fractional bias, moderate reductions in fractional error, and improved correlations for all species. Results from the leave-one-out and 10-fold CV are nearly identical. Random folding may not provide additional insights beyond the leave-one-out CV, because ground-level monitors tend to be clustered in metropolitan areas. Therefore, the regional holdout CV is helpful in evaluating model performance when extrapolating to regions with fewer monitors, which tend to be remote. GWR performance does degrade with the regional holdout CV, but it still yields significant improvements over the uncorrected CTM despite the 400 km radius holdout. This suggests that GWR performance is potentially weaker in remote regions, compared to urban areas. However, epidemiological analyses would be less sensitive to estimates in remote regions due to lower population densities.

We also compare visual patterns in the observed and predicted biases to provide an additional, albeit qualitative, point of comparison. CTM biases calculated at monitor locations (i.e., observed biases) and those predicted by GWR models are shown in Figures 4 and 5, respectively. In general, the GWR models replicate spatial patterns in observed biases. Biases for EC tend to be negligible or slightly negative in remote areas and positive in select metropolitan areas. In 2001, positive EC biases are observed in a greater number of metropolitan areas, resulting in positive bias predictions in the Midwest and eastern coast. Biases for OA are negative in the western U.S., particularly in the California central valley and positive in the eastern coast. For 2010, in particular, OA is overpredicted in the southeastern U.S., where biogenic emissions contribute significantly to OA production. In 2001, the OA bias in the southeast may not be as severe due to higher anthropogenic emissions that partially offset the bias, or due to insufficient monitors. Biases for NO_3^- are negative in the western U.S., particularly in the California central valley, and positive in the eastern U.S. For 2001, predicted NO_3^- biases in the Midwest are highly dissimilar, which may be due to the lack of monitors in the region. Under these condition, GWR models would assign equal weighting to western and eastern monitors, potentially causing this dissimilarity. In 2010, the introduction of new monitors in the region shows that biases in the Midwest tend to be negative, which is reflected in the predicted biases. Biases of SO_4^{2-} are relatively mild, but tend to be negative in the eastern U.S. and California central valley, and positive in the western U.S. Likewise, biases for NH_4^+ are relatively mild, and tend to mirror the patterns observed for SO_4^{2-}, except in the southeast. Since NH_4^+ neutralizes both NO_3^- and SO_4^{2-}, positive biases for NO_3^- in the southeast may also lead to positive biases for NH_4^+. Corrected species are reconstructed in the rightmost panel of Figure 1, with crustal PM and sea salt still omitted. For both simulation years, the bias-corrected CTM estimates continue to be biased low, due to the omission of crustal PM and sea salt, but the bias is relatively uniform and no longer characterized by severe regional variations. GWR corrections improve the spatial consistency of CTM estimates and make them viable for exposure assignment in epidemiological studies.

Compositional Evaluation

Some applications of the predicted composition fields may use the fractional composition of the $PM_{2.5}$ rather than the speciated concentrations themselves. Therefore, as an additional point of evaluation, the fractional composition of simulated $PM_{2.5}$ is compared to that observed in speciated ground-level monitors. Here, we are interested in examining the CTM's performance to predict species mixtures on a relative basis and improvements made by GWR corrections. Fractional composition can be represented as a vector, where each dimension corresponds to the fractional contribution of a species. The degree of dissimilarity between species mixtures can be quantified by calculating the angle between their corresponding vectors. For reference, Figure S1 compares example monitor and CTM species mixtures with vector angles of 5, 10, 20 and 30 degrees between them. A vector angle below 10 degrees is classified as showing good agreement between simulated and observed species mixtures. Changes in vector angles before and after GWR corrections are shown in Figure 6, with 10-fold CV results being presented. Figure 6 a) highlights a clear shift in the distribution of vector angles, with an average decrease of 2.3 and 5.5 degrees in 2001 and 2010, respectively. In 2001, the number of monitor locations with vector angles under 10 degrees increases from 56 to 70% as a result of GWR corrections. In 2010, the increase is greater, from 32 to 80%. Changes to vector angles at individual monitor locations are more clearly represented in Figure 6 b). In general, corrected estimates in eastern locations agree better with monitors than those in western locations. GWR corrections also improve agreement between CTM and CSN monitors. However, there appears to be a degradation in performance at some western IMPROVE locations. This is consistent with earlier results showing persistent error after corrections are applied to western OA and NO_3^- estimates, and regional holdout CV results that suggest weaker predictive ability in remote regions.

Impact of Spatial Aggregation

We intentionally developed exposure estimates to be easily used in various census geographies that are commonly used in assignments of $PM_{2.5}$ exposures. In Figure S2, we reconstruct corrected $PM_{2.5}$, without crustal PM and sea salt, and compare directly to IEG estimates at tract-, county- and MSA-level resolutions. Modest improvements in correlations and RMSE from tract level to county level suggest that spatial aggregation may potentially reduce some noise in the corrected estimates. Additionally, we note that the corrected CTM remains biased low relative to IEG estimates, as a result of omitting crustal PM and sea salt.

Indirect Changes to Source Mixtures

The nation-wide network of speciated ground-level $PM_{2.5}$ monitors provide critical information on chemical composition, which is the basis for the corrections performed in this study. However, there are no data sources that detail the source apportionment of $PM_{2.5}$ on a national scale. Therefore, analogous corrections to the source-resolution of $PM_{2.5}$ are not possible. Instead, for each species, we preserve the original source mixture, as predicted by the CTM, in our corrected estimates. The fractional source mixture is calculated for each simulated $PM_{2.5}$ species, and simply re-applied to the corrected estimates. However, because the quantity of each species has been adjusted, the source mixture for total $PM_{2.5}$ is altered by GWR corrections. Figure S3 illustrates the changes in relative source mixture for each source category. In general, the changes to source mixture are minimal, with the exception of the on-road and non-road source categories. GWR correction increases the contribution from on-road and non-road emissions in the west by approximately 50%. This is primarily due to the increase in NO_3^- in corrected CTM simulations. On-road and non-road emissions tend to be concentrated in specific locations (e.g., roadways). Coupled with complex terrain in the western U.S., NO_3^- emissions gradients tend to be large and poorly represented in coarse 36 km resolution grids. As a result, NO_3^- from mobile sources are under-predicted by the CTM, an error that is indirectly adjusted by GWR corrections.

Conclusion

In this paper, we present $PM_{2.5}$ exposure estimates resolved by species and source for 2001 and 2010 across the continental U.S. GWR corrections improve the spatial consistency of CTM simulations by leveraging valuable information from monitors, empirical estimates and other land use variables. In particular, significant improvements are made for estimates of EC, OA and NO_3^-, which correct a significant portion of the initial error and bias in total $PM_{2.5}$ estimates from the CTM. Going forward, we hope this enables CTMs to be more widely used for predictions, such as $PM_{2.5}$ source, that are unavailable elsewhere at the same scale. The use of geostatistical methods, including but not limited to GWR, should also be considered when processing CTM simulations, with the aim of improving and further evaluating said estimates.

Acknowledgements: This publication was developed as part of the Center for Air, Climate, and Energy Solutions (CACES), which was supported under Assistance Agreement No. R835873 awarded by the U.S. Environmental Protection Agency. It has not been formally reviewed by EPA. The views expressed in this document are solely those of authors and do not necessarily reflect those of the Agency. EPA does not endorse any products or commercial services mentioned in this publication.

Tables and Figures

Year	Species	CSN	IMPROVE	Total
2001	EC	28	92	120
2010	EC	151	147	298
2001	OM	27	92	119
2010	OM	153	145	298
2001	NH_4	20	91	111
2010	NH_4	174	146	320
2001	NO_3	20	91	111
2010	NO_3	168	145	313
2001	SO_4	21	91	112
2010	SO_4	175	146	321
2001	Co-located*	18	91	109
2010	Co-located*	140	144	284

Table 1. Number of speciated monitors used in observational dataset. Data broken down by year, $PM_{2.5}$ species and monitoring network. *Number of instances where all 5 species are measured at the same monitoring location.

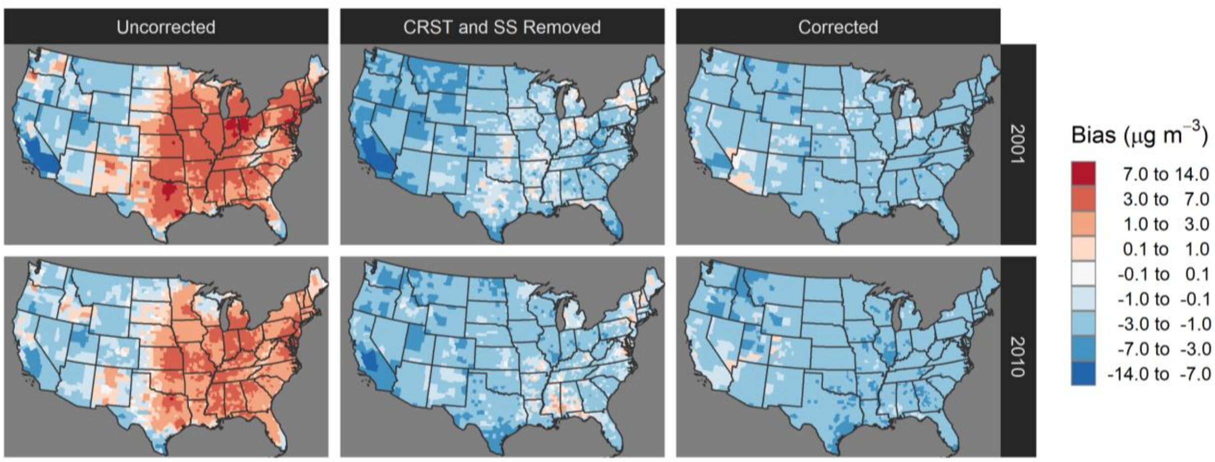

Figure 1. Bias of CTM-predicted $PM_{2.5}$ relative to IEG-predicted $PM_{2.5}$ (i.e., CTM – IEG). Left-hand panel shows uncorrected CTM predictions, middle panel shows uncorrected CTM predictions without crustal PM and sea salt, right-hand panel shows corrected CTM predictions without crustal PM and sea salt. Top and bottom rows show annually-averaged biases for 2001 and 2010 predictions, respectively. Biases are county-level population-weighted averages.

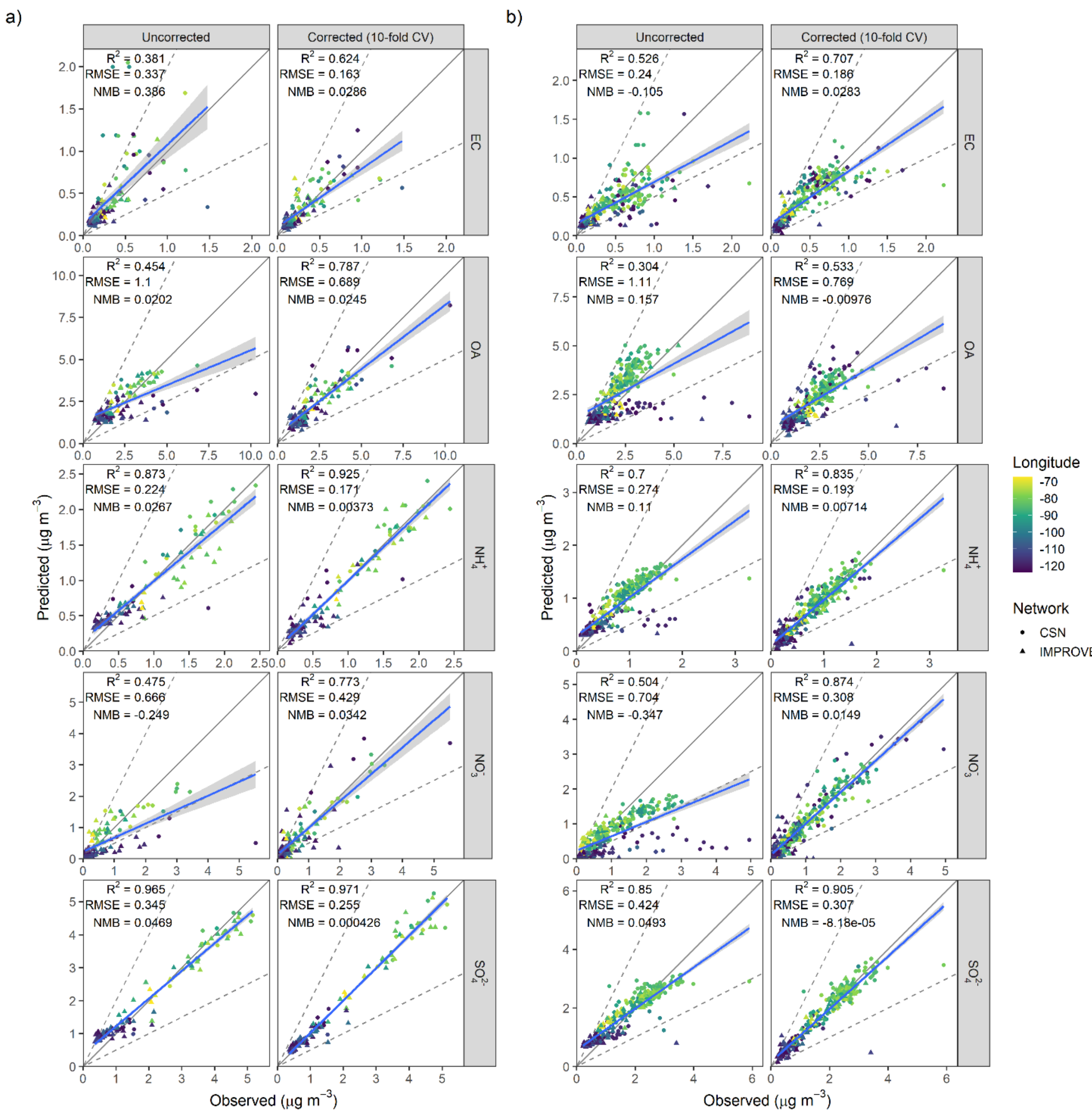

Figure 2. Evaluation of CTM-predicted $PM_{2.5}$ species against observations from speciated ground-level monitors. Figures a) and b) show evaluations of 2001 and 2010 simulation years, respectively. Values shown are annual-averages at monitor locations. RMSE represents the root mean square error. NMB represents the normalized mean bias. Solid lines denote a 1:1 slope. Dashed lines denote a 1:2 or 2:1 slope.

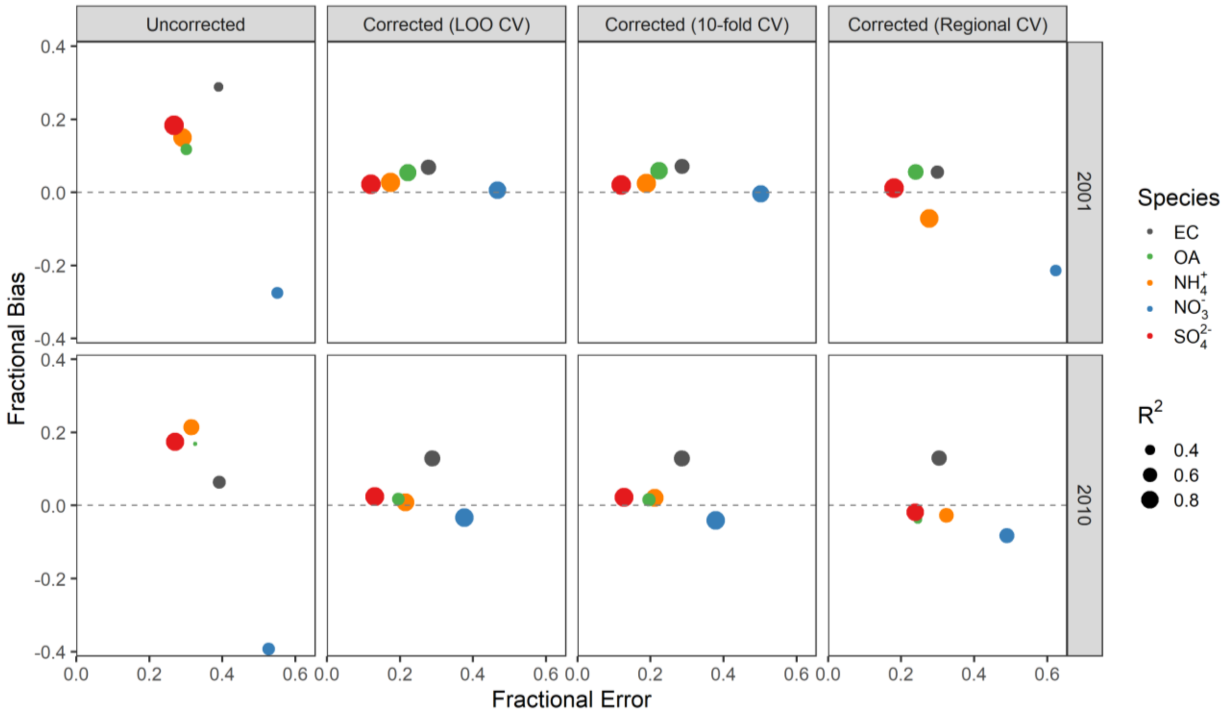

Figure 3. Summary of CTM evaluations for uncorrected and GWR-corrected simulations trained under leave-one-out (LOO), 10-fold and regional cross-validation (CV) methods. Evaluation metrics are calculated for individual $PM_{2.5}$ species across the continental U.S.

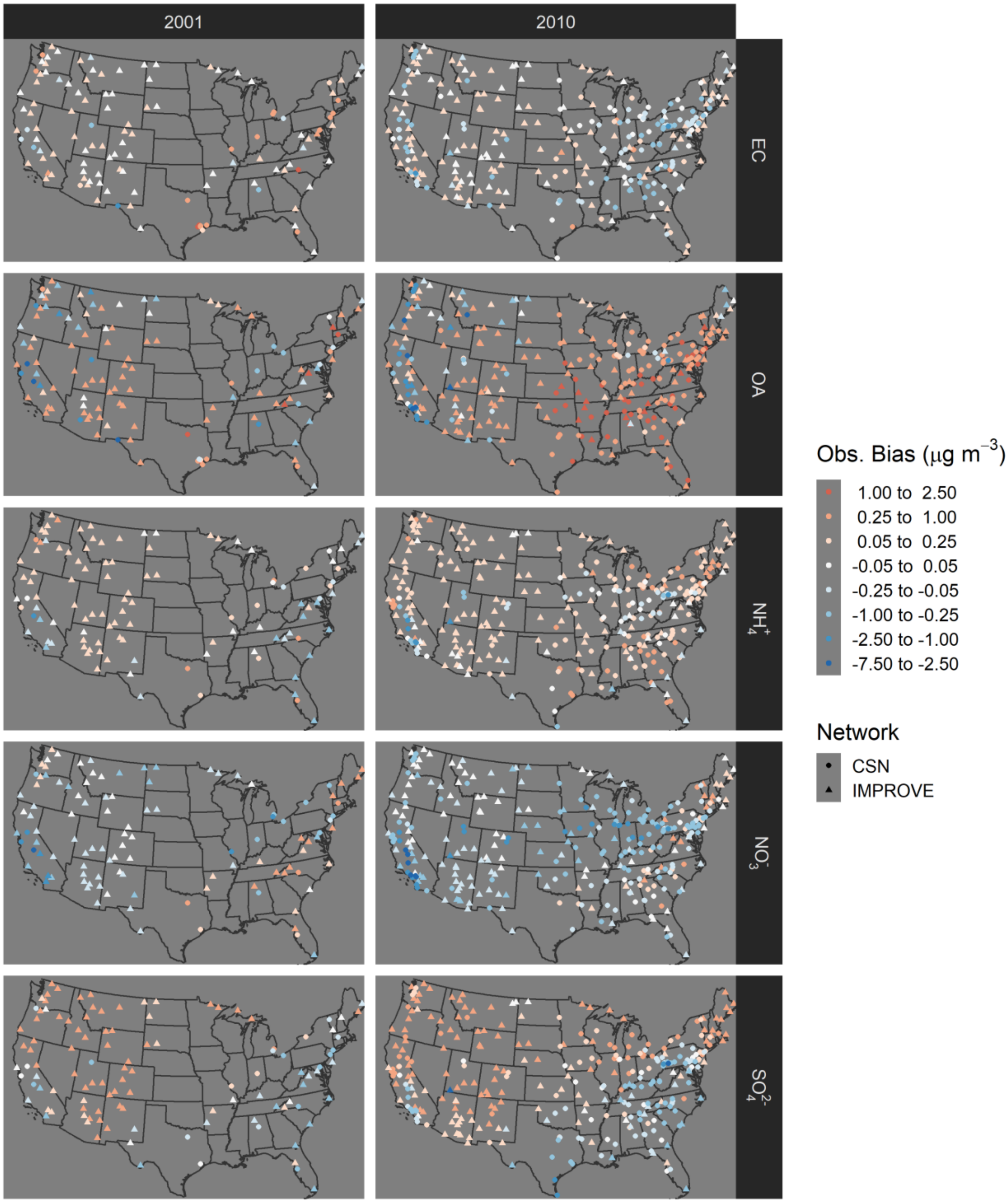

Figure 4. Bias of uncorrected CTM $PM_{2.5}$ species relative to observations at speciated ground-level monitors (observed bias).

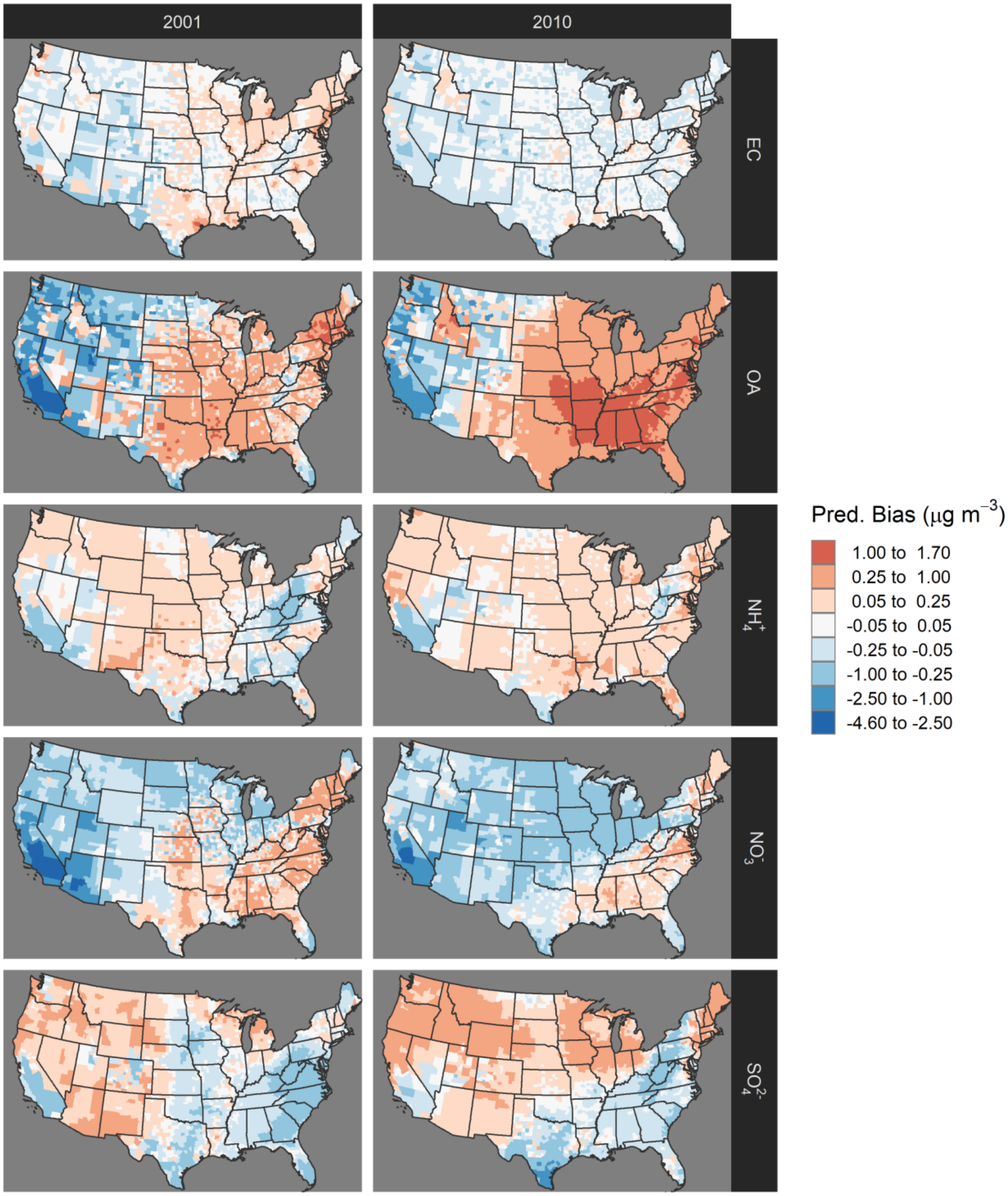

Figure 5. Bias of CTM $PM_{2.5}$ species as predicted by GWR models (predicted bias). Values shown are county-level population-weighted averages.

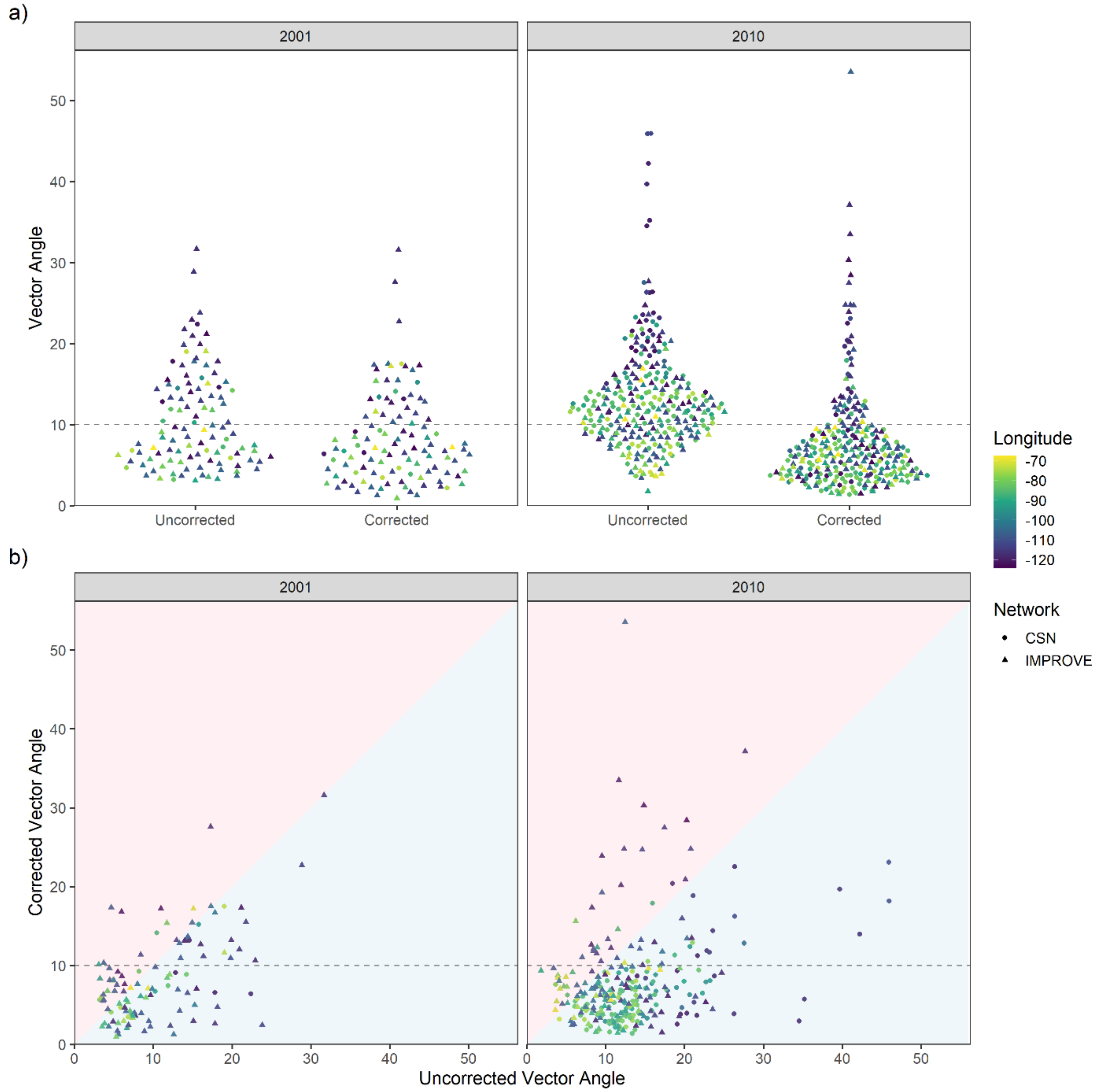

Figure 6. Evaluation of vector angles before and after GWR correction. Vector angles are calculated when speciated monitors for EC, OC, NH_4^+, NO_3^-, and SO_4^{2-} are all present. Corrected vector angles are based on results from the 10-fold cross-validation. Figure a) illustrates the change in vector angle distributions. Figure b) directly compares uncorrected and corrected vector angles. Red areas denote an increase in the vector angle. Blue areas denote a decrease in the vector angle.

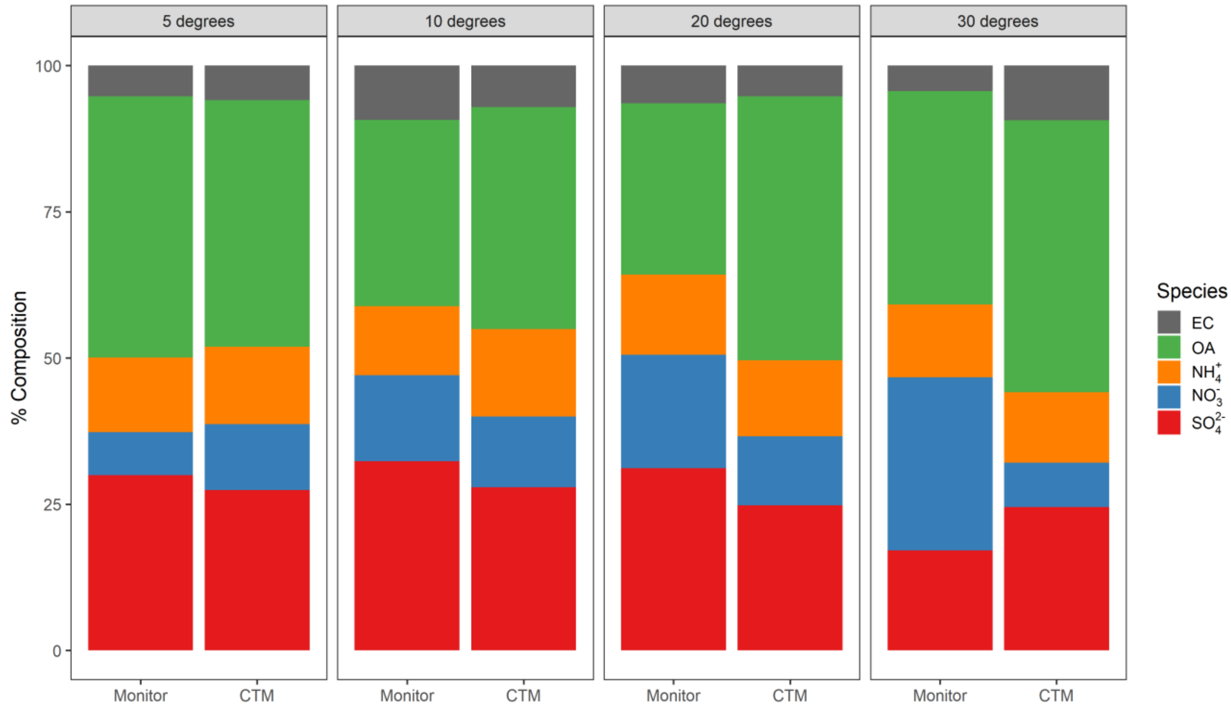

Figure S1. Illustrative example of vector angles between monitor and CTM species mixtures. A vector angle of zero indicates equivalent species mixtures. Vector angle increases as species mixtures become more dissimilar.

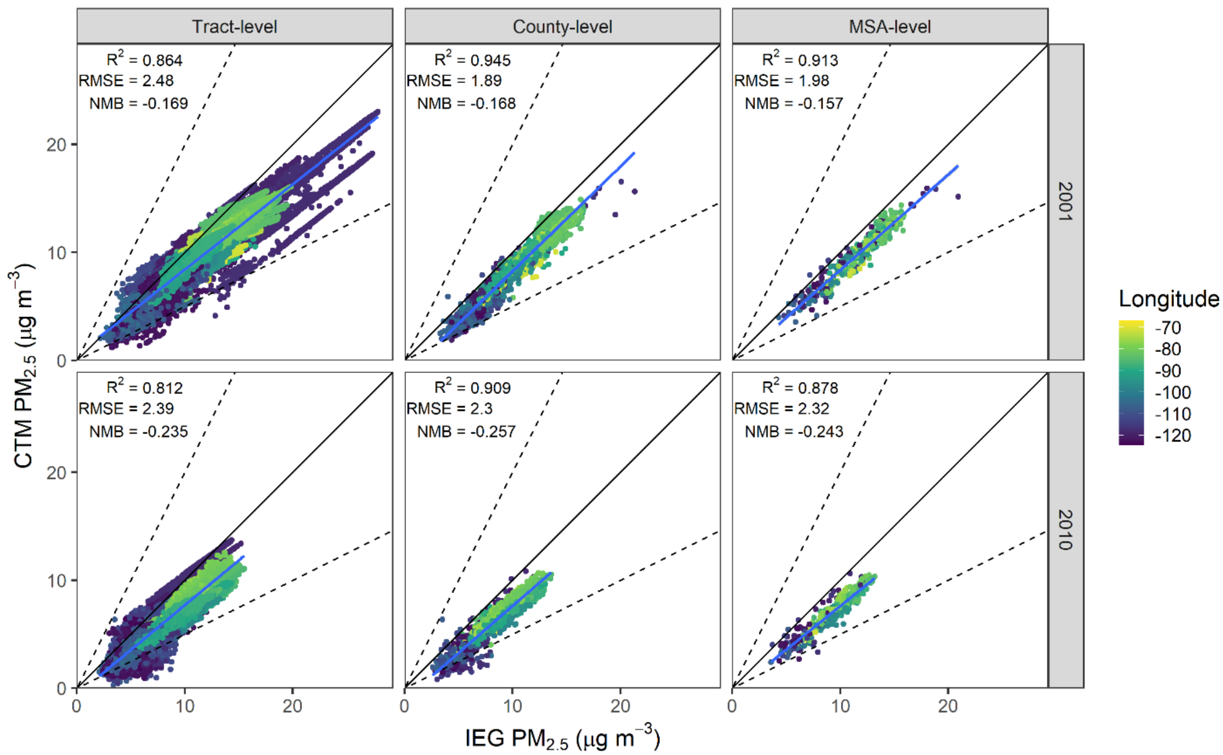

Figure S2. Effect of spatial aggregation on GWR-corrected CTM predictions. CTM $PM_{2.5}$ is reconstructed from the sum of GWR-corrected EC, OC, NH_4^+, NO_3^-, and SO_4^{2-}. CTM predictions are compared against IEG model predictions. All values are annual-averages. County-level and MSA-level values are population-weighted averages. Solid lines denote a 1:1 slope. Dashed lines denote a 1:2 or 2:1 slope.

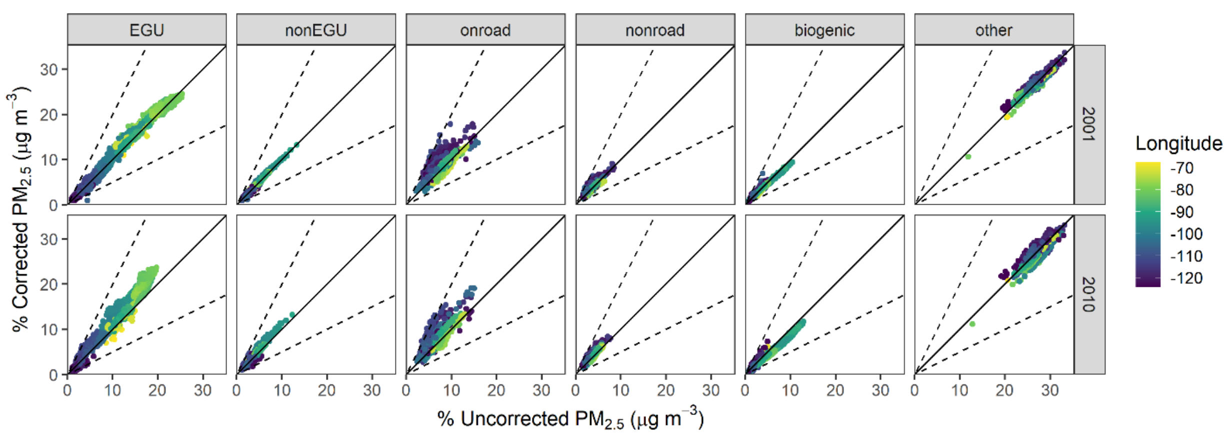

Figure S3. Indirect changes to source mixtures resulting from GWR corrections. Data points represent annually-averaged source mixtures at the county-level after population-weighted averaging. Solid lines denote a 1:1 slope. Dashed lines denote a 1:2 or 2:1 slope.

References

1. Amante, C.; Eakins B. W. ETOPO1 1 Arc-Minute Global Relief Model: Procedures, Data Sources and Analysis. NOAA Technical Memorandum NESDIS NGDC-24. National Geophysical Data Center 2009. https://doi:10.7289/V5C8276M.
2. Appel, K. W.; Pouliot, G. A.; Simon, H.; Sarwar, G.; Pye, H. O. T.; Napelenok, S. L.; Akhtar, F.; Roselle, S. J. Evaluation of Dust and Trace Metal Estimates from the Community Multiscale Air Quality (CMAQ) Model Version 5.0. Geosci. Model Dev. 2013, 6 (4), 883–899. https://doi.org/10.5194/gmd-6-883-2013.
3. Apte, J. S.; Brauer, M.; Cohen, A. J.; Ezzati, M.; Pope, C. A. Ambient PM2.5 Reduces Global and Regional Life Expectancy. Environ. Sci. Technol. Lett. 2018, 5 (9), 546–551. https://doi.org/10.1021/acs.estlett.8b00360.
4. Bennett, J. E.; Tamura-Wicks, H.; Parks, R. M.; Burnett, R. T.; Pope, C. A.; Bechle, M. J.; Marshall, J. D.; Danaei, G.; Ezzati, M. Particulate Matter Air Pollution and National and County Life Expectancy Loss in the USA: A Spatiotemporal Analysis. PLoS Med 2019, 16 (7), e1002856. https://doi.org/10.1371/journal.pmed.1002856.
5. Berrocal, V. J.; Guan, Y.; Muyskens, A.; Wang, H.; Reich, B. J.; Mulholland, J. A.; Chang, H. H. A Comparison of Statistical and Machine Learning Methods for Creating National Daily Maps of Ambient PM2.5 Concentration. Atmospheric Environment 2020, 222, 117130. https://doi.org/10.1016/j.atmosenv.2019.117130.
6. Brunsdon, C.; Fotheringham, A. S.; Charlton, M. E. Geographically Weighted Regression: A Method for Exploring Spatial Nonstationarity. Geographical Analysis 1996, 28 (4), 281–298. https://doi.org/10.1111/j.1538-4632.1996.tb00936.x.
7. Cohen, A. J.; Brauer, M.; Burnett, R.; Anderson, H. R.; Frostad, J.; Estep, K.; Balakrishnan, K.; Brunekreef, B.; Dandona, L.; Dandona, R.; Feigin, V.; Freedman, G.; Hubbell, B.; Jobling, A.; Kan, H.; Knibbs, L.; Liu, Y.; Martin, R.; Morawska, L.; Pope, C. A.; Shin, H.; Straif, K.; Shaddick, G.; Thomas, M.; van Dingenen, R.; van Donkelaar, A.; Vos, T.; Murray, C. J. L.; Forouzanfar, M. H. Estimates and 25-Year Trends of the Global Burden of Disease Attributable to Ambient Air Pollution: An Analysis of Data from the Global Burden of Diseases Study 2015. The Lancet 2017, 389 (10082), 1907–1918. https://doi.org/10.1016/S0140-6736(17)30505-6.
8. Correia, A. W.; Pope, C. A.; Dockery, D. W.; Wang, Y.; Ezzati, M.; Dominici, F. Effect of Air Pollution Control on Life Expectancy in the United States: An Analysis of 545 U.S. Counties for the Period from 2000 to 2007. Epidemiology 2013, 24 (1), 23–31. https://doi.org/10.1097/EDE.0b013e3182770237.

9. Donahue, N. M.; Robinson, A. L.; Stanier, C. O.; Pandis, S. N. Coupled Partitioning, Dilution, and Chemical Aging of Semivolatile Organics. Environmental Science & Technology 2006, 40 (8), 2635–2643. https://doi.org/10.1021/es052297c.
10. Friedl, M.; Sulla-Menashe, D. MCD12Q1 MODIS/Terra+Aqua Land Cover Type Yearly L3 Global 500m SIN Grid V006. NASA EOSDIS Land Processes DAAC 2019. https://doi.org/10.5067/MODIS/MCD12Q1.006
11. Geng, G.; Zhang, Q.; Martin, R. V.; van Donkelaar, A.; Huo, H.; Che, H.; Lin, J.; He, K. Estimating Long-Term PM2.5 Concentrations in China Using Satellite-Based Aerosol Optical Depth and a Chemical Transport Model. Remote Sensing of Environment 2015, 166, 262–270. https://doi.org/10.1016/j.rse.2015.05.016.
12. Geng, G.; Zhang, Q.; Tong, D.; Li, M.; Zheng, Y.; Wang, S.; He, K. Chemical Composition of Ambient PM2.5 over China and Relationship to Precursor Emissions during 2005–2012. Atmospheric Chemistry and Physics 2017, 17 (14), 9187–9203. https://doi.org/10.5194/acp-17-9187-2017.
13. Hammer, M. S.; van Donkelaar, A.; Li, C.; Lyapustin, A.; Sayer, A. M.; Hsu, N. C.; Levy, R. C.; Garay, M. J.; Kalashnikova, O. V.; Kahn, R. A.; Brauer, M.; Apte, J. S.; Henze, D. K.; Zhang, L.; Zhang, Q.; Ford, B.; Pierce, J. R.; Martin, R. V. Global Estimates and Long-Term Trends of Fine Particulate Matter Concentrations (1998–2018). Environ. Sci. Technol. 2020, 54 (13), 7879–7890. https://doi.org/10.1021/acs.est.0c01764.
14. Harrison, R. M.; Yin, J. Particulate Matter in the Atmosphere: Which Particle Properties Are Important for Its Effects on Health? Science of The Total Environment 2000, 249 (1–3), 85–101. https://doi.org/10.1016/S0048-9697(99)00513-6.
15. Hu, X.; Waller, L. A.; Al-Hamdan, M. Z.; Crosson, W. L.; Estes, M. G.; Estes, S. M.; Quattrochi, D. A.; Sarnat, J. A.; Liu, Y. Estimating Ground-Level PM2.5 Concentrations in the Southeastern U.S. Using Geographically Weighted Regression. Environmental Research 2013, 121, 1–10. https://doi.org/10.1016/j.envres.2012.11.003.
16. Hu, Z. Spatial Analysis of MODIS Aerosol Optical Depth, PM2.5, and Chronic Coronary Heart Disease. International Journal of Health Geographics 2009, 8 (1), 27. https://doi.org/10.1186/1476-072X-8-27.
17. Huang, C.; Hu, J.; Xue, T.; Xu, H.; Wang, M. High-Resolution Spatiotemporal Modeling for Ambient PM2.5 Exposure Assessment in China from 2013 to 2019. Environ. Sci. Technol. 2021, 55 (3), 2152–2162. https://doi.org/10.1021/acs.est.0c05815.
18. Karydis, V. A.; Tsimpidi, A. P.; Fountoukis, C.; Nenes, A.; Zavala, M.; Lei, W.; Molina, L. T.; Pandis, S. N. Simulating the Fine and Coarse Inorganic Particulate Matter Concentrations in a

Polluted Megacity. Atmospheric Environment 2010, 44 (5), 608–620. https://doi.org/10.1016/j.atmosenv.2009.11.023.

19. Kelly, F. J.; Fussell, J. C. Size, Source and Chemical Composition as Determinants of Toxicity Attributable to Ambient Particulate Matter. Atmospheric Environment 2012, 60, 504–526. https://doi.org/10.1016/j.atmosenv.2012.06.039.
20. Kim, S.-Y.; Bechle, M.; Hankey, S.; Sheppard, L.; Szpiro, A. A.; Marshall, J. D. Concentrations of Criteria Pollutants in the Contiguous U.S., 1979 – 2015: Role of Prediction Model Parsimony in Integrated Empirical Geographic Regression. PLOS ONE 2020, 15 (2), e0228535. https://doi.org/10.1371/journal.pone.0228535.
21. Lee, S.-J.; Serre, M. L.; van Donkelaar, A.; Martin, R. V.; Burnett, R. T.; Jerrett, M. Comparison of Geostatistical Interpolation and Remote Sensing Techniques for Estimating Long-Term Exposure to Ambient PM2.5 Concentrations across the Continental United States. Environmental Health Perspectives 2012, 120 (12), 1727–1732. https://doi.org/10.1289/ehp.1205006.
22. Lefler, J. S.; Higbee, J. D.; Burnett, R. T.; Ezzati, M.; Coleman, N. C.; Mann, D. D.; Marshall, J. D.; Bechle, M.; Wang, Y.; Robinson, A. L.; Arden Pope, C. Air Pollution and Mortality in a Large, Representative U.S. Cohort: Multiple-Pollutant Analyses, and Spatial and Temporal Decompositions. Environmental Health 2019, 18 (1), 101. https://doi.org/10.1186/s12940-019-0544-9.
23. Li, C.; Martin, R. V.; van Donkelaar, A.; Boys, B. L.; Hammer, M. S.; Xu, J.-W.; Marais, E. A.; Reff, A.; Strum, M.; Ridley, D. A.; Crippa, M.; Brauer, M.; Zhang, Q. Trends in Chemical Composition of Global and Regional Population-Weighted Fine Particulate Matter Estimated for 25 Years. Environmental Science & Technology 2017b, 51 (19), 11185–11195. https://doi.org/10.1021/acs.est.7b02530.
24. Li, T.; Shen, H.; Zeng, C.; Yuan, Q.; Zhang, L. Point-Surface Fusion of Station Measurements and Satellite Observations for Mapping PM2.5 Distribution in China: Methods and Assessment. Atmospheric Environment 2017a, 152, 477–489. https://doi.org/10.1016/j.atmosenv.2017.01.004.
25. Lordo, R.; Landis, E.; Rice, J.; Triplett, C. Assessing the Statistical Relationship in Carbon Measurements Between Old and New Sampling and Analysis Protocols in the Chemical Speciation Network (CSN). A Presentation to the 2016 National Ambient Air Monitoring Conference.
26. Lyu, B.; Hu, Y.; Zhang, W.; Du, Y.; Luo, B.; Sun, X.; Sun, Z.; Deng, Z.; Wang, X.; Liu, J.; Wang, X.; Russell, A. G. Fusion Method Combining Ground-Level Observations with Chemical Transport Model Predictions Using an Ensemble Deep Learning Framework: Application in

China to Estimate Spatiotemporally-Resolved PM2.5 Exposure Fields in 2014–2017. Environ. Sci. Technol. 2019, 53 (13), 7306–7315. https://doi.org/10.1021/acs.est.9b01117.

27. Ma, Z.; Hu, X.; Huang, L.; Bi, J.; Liu, Y. Estimating Ground-Level PM2.5 in China Using Satellite Remote Sensing. Environ. Sci. Technol. 2014, 48 (13), 7436–7444. https://doi.org/10.1021/es5009399.
28. Malm, W. C.; Schichtel, B. A.; Pitchford, M. L. Uncertainties in PM2.5 Gravimetric and Speciation Measurements and What We Can Learn from Them. Journal of the Air & Waste Management Association 2011, 61 (11), 1131–1149. https://doi.org/10.1080/10473289.2011.603998.
29. Meng, J.; Li, C.; Martin, R. V.; van Donkelaar, A.; Hystad, P.; Brauer, M. Estimated Long-Term (1981–2016) Concentrations of Ambient Fine Particulate Matter across North America from Chemical Transport Modeling, Satellite Remote Sensing, and Ground-Based Measurements. Environmental Science & Technology 2019, 53 (9), 5071–5079. https://doi.org/10.1021/acs.est.8b06875.
30. Murphy, B. N.; Pandis, S. N. Simulating the Formation of Semivolatile Primary and Secondary Organic Aerosol in a Regional Chemical Transport Model. Environmental Science & Technology 2009, 43 (13), 4722–4728. https://doi.org/10.1021/es803168a.
31. Murphy, B. N.; Pandis, S. N. Exploring Summertime Organic Aerosol Formation in the Eastern United States Using a Regional-Scale Budget Approach and Ambient Measurements: Organic Aerosol Budget in the Easter United States. Journal of Geophysical Research: Atmospheres 2010, 115 (D24). https://doi.org/10.1029/2010JD014418.
32. NOAA National Geophysical Data Center. ETOPO1 1 Arc-Minute Global Relief Model. NOAA National Centers for Environmental Information 2009.
33. Philip, S.; Martin, R. V.; van Donkelaar, A.; Lo, J. W.-H.; Wang, Y.; Chen, D.; Zhang, L.; Kasibhatla, P. S.; Wang, S.; Zhang, Q.; Lu, Z.; Streets, D. G.; Bittman, S.; Macdonald, D. J. Global Chemical Composition of Ambient Fine Particulate Matter for Exposure Assessment. Environmental Science & Technology 2014, 48 (22), 13060–13068. https://doi.org/10.1021/es502965b.
34. Pope, C. A.; Coleman, N.; Pond, Z. A.; Burnett, R. T. Fine Particulate Air Pollution and Human Mortality: 25+ Years of Cohort Studies. Environmental Research 2020, 183, 108924. https://doi.org/10.1016/j.envres.2019.108924.
35. Pope, C. A.; Dockery, D. W. Health Effects of Fine Particulate Air Pollution: Lines That Connect. Journal of the Air & Waste Management Association 2006, 56 (6), 709–742. https://doi.org/10.1080/10473289.2006.10464485.

36. Pope III, C. A.; Ezzati, M.; Dockery, D. W. Fine-Particulate Air Pollution and Life Expectancy in the United States. New England Journal of Medicine 2009, 11.
37. Posner, L. N.; Theodoritsi, G.; Robinson, A.; Yarwood, G.; Koo, B.; Morris, R.; Mavko, M.; Moore, T.; Pandis, S. N. Simulation of Fresh and Chemically-Aged Biomass Burning Organic Aerosol. Atmospheric Environment 2019, 196, 27–37. https://doi.org/10.1016/j.atmosenv.2018.09.055.
38. R Core Team. R: A Language and Environment for Statistical Computing. R Foundation for Statistical Computing, Vienna, Austria 2021. https://www.R-project.org/.
39. Robinson, A. L.; Donahue, N. M.; Shrivastava, M. K.; Weitkamp, E. A.; Sage, A. M.; Grieshop, A. P.; Lane, T. E.; Pierce, J. R.; Pandis, S. N. Rethinking Organic Aerosols: Semivolatile Emissions and Photochemical Aging. Science 2007, 315 (5816), 1259–1262. https://doi.org/10.1126/science.1133061.
40. Skyllakou, K.; Murphy, B. N.; Megaritis, A. G.; Fountoukis, C.; Pandis, S. N. Contributions of Local and Regional Sources to Fine PM in the Megacity of Paris. Atmospheric Chemistry and Physics 2014, 14 (5), 2343–2352. https://doi.org/10.5194/acp-14-2343-2014.
41. Skyllakou, K.; Fountoukis, C.; Charalampidis, P.; Pandis, S. N. Volatility-Resolved Source Apportionment of Primary and Secondary Organic Aerosol over Europe. Atmospheric Environment 2017, 167, 1–10. https://doi.org/10.1016/j.atmosenv.2017.08.005.
42. Skyllakou, K.; Garcia Rivera, P.; Dinkelacker, B.; Karnezi, E.; Kioutsioukis, I.; Hernandez, C.; Adams, P. J.; Pandis, S. N. Changes in PM2.5 concentrations and their sources in the US from 1990 to 2010. Atmos. Chem. Phys. Discuss. [preprint] 2021, in review. https://doi.org/10.5194/acp-2021-495.
43. Solomon, P. A.; Crumpler, D.; Flanagan, J. B.; Jayanty, R. K. M.; Rickman, E. E.; McDade, C. E. U.S. National PM2.5 Chemical Speciation Monitoring Networks—CSN and IMPROVE: Description of Networks. Journal of the Air & Waste Management Association 2014, 64 (12), 1410–1438. https://doi.org/10.1080/10962247.2014.956904.
44. Song, W.; Jia, H.; Huang, J.; Zhang, Y. A Satellite-Based Geographically Weighted Regression Model for Regional PM2.5 Estimation over the Pearl River Delta Region in China. Remote Sensing of Environment 2014, 154, 1–7. https://doi.org/10.1016/j.rse.2014.08.008.
45. Spada, N. J.; Hyslop, N. P. Comparison of Elemental and Organic Carbon Measurements between IMPROVE and CSN before and after Method Transitions. Atmospheric Environment 2018, 178, 173–180. https://doi.org/10.1016/j.atmosenv.2018.01.043.

46. Tsimpidi, A. P.; Karydis, V. A.; Zavala, M.; Lei, W.; Molina, L.; Ulbrich, I. M.; Jimenez, J. L.; Pandis, S. N. Evaluation of the Volatility Basis-Set Approach for the Simulation of Organic Aerosol Formation in the Mexico City Metropolitan Area. Atmos. Chem. Phys. 2010, 22.
47. U.S. Environmental Protection Agency. The Benefits and Costs of the Clean Air Act, 1990 to 2010; Office of Air and Radiation: Washington D.C., 1999.
48. U.S. Environmental Protection Agency. The Benefits and Costs of the Clean Air Act from 1990 to 2020; Office of Air and Radiation: Washington D.C., 2011.
49. U.S. Environmental Protection Agency. Regulatory Impact Analysis for the Final Revisions to the National Ambient Air Quality Standards for Particulate Matter; Office of Air Quality Planning and Standards: Research Triangle Park, NC, 2012.
50. van Donkelaar, A.; Martin, R. V.; Spurr, R. J. D.; Burnett, R. T. High-Resolution Satellite-Derived PM2.5 from Optimal Estimation and Geographically Weighted Regression over North America. Environmental Science & Technology 2015, 49 (17), 10482–10491. https://doi.org/10.1021/acs.est.5b02076.
51. van Donkelaar, A.; Martin, R. V.; Brauer, M.; Hsu, N. C.; Kahn, R. A.; Levy, R. C.; Lyapustin, A.; Sayer, A. M.; Winker, D. M. Global Estimates of Fine Particulate Matter Using a Combined Geophysical-Statistical Method with Information from Satellites, Models, and Monitors. Environmental Science & Technology 2016, 50 (7), 3762–3772. https://doi.org/10.1021/acs.est.5b05833.
52. van Donkelaar, A.; Martin, R. V.; Li, C.; Burnett, R. T. Regional Estimates of Chemical Composition of Fine Particulate Matter Using a Combined Geoscience-Statistical Method with Information from Satellites, Models, and Monitors. Environmental Science & Technology 2019, 53 (5), 2595–2611. https://doi.org/10.1021/acs.est.8b06392.
53. Wagstrom, K. M.; Pandis, S. N. Contribution of Long Range Transport to Local Fine Particulate Matter Concerns. Atmospheric Environment 2011, 45 (16), 2730–2735. https://doi.org/10.1016/j.atmosenv.2011.02.040.
54. Wagstrom, K. M.; Pandis, S. N. Source–Receptor Relationships for Fine Particulate Matter Concentrations in the Eastern United States. Atmospheric Environment 2011, 45 (2), 347–356. https://doi.org/10.1016/j.atmosenv.2010.10.019.
55. Wagstrom, K. M.; Pandis, S. N.; Yarwood, G.; Wilson, G. M.; Morris, R. E. Development and Application of a Computationally Efficient Particulate Matter Apportionment Algorithm in a Three-Dimensional Chemical Transport Model. Atmospheric Environment 2008, 42 (22), 5650–5659. https://doi.org/10.1016/j.atmosenv.2008.03.012.

56. Wang, M.; Sampson, P. D.; Hu, J.; Kleeman, M.; Keller, J. P.; Olives, C.; Szpiro, A. A.; Vedal, S.; Kaufman, J. D. Combining Land-Use Regression and Chemical Transport Modeling in a Spatiotemporal Geostatistical Model for Ozone and PM2.5. Environ. Sci. Technol. 2016, 50 (10), 5111–5118. https://doi.org/10.1021/acs.est.5b06001.
57. Xing, J.; Pleim, J.; Mathur, R.; Pouliot, G.; Hogrefe, C.; Gan, C.-M.; Wei, C. Historical Gaseous and Primary Aerosol Emissions in the United States from 1990 to 2010. Atmospheric Chemistry and Physics 2013, 13 (15), 7531–7549. https://doi.org/10.5194/acp-13-7531-2013.
58. Xu, J.-W.; Martin, R. V.; Henderson, B. H.; Meng, J.; Öztaner, Y. B.; Hand, J. L.; Hakami, A.; Strum, M.; Phillips, S. B. Simulation of Airborne Trace Metals in Fine Particulate Matter over North America. Atmospheric Environment 2019, 214, 116883. https://doi.org/10.1016/j.atmosenv.2019.116883.
59. You, W.; Zang, Z.; Zhang, L.; Li, Y.; Pan, X.; Wang, W. National-Scale Estimates of Ground-Level PM2.5 Concentration in China Using Geographically Weighted Regression Based on 3 Km Resolution MODIS AOD. Remote Sensing 2016, 8 (3), 184. https://doi.org/10.3390/rs8030184.
60. Zhai, L.; Li, S.; Zou, B.; Sang, H.; Fang, X.; Xu, S. An Improved Geographically Weighted Regression Model for PM2.5 Concentration Estimation in Large Areas. Atmospheric Environment 2018, 181, 145–154. https://doi.org/10.1016/j.atmosenv.2018.03.017.
61. Zhang, Y.; West, J. J.; Mathur, R.; Xing, J.; Hogrefe, C.; Roselle, S. J.; Bash, J. O.; Pleim, J. E.; Gan, C.-M.; Wong, D. C. Long-Term Trends in the Ambient PM2.5- and O3-Related Mortality Burdens in the United States under Emission Reductions from 1990 to 2010. Atmospheric Chemistry and Physics 2018, 18 (20), 15003–15016. https://doi.org/10.5194/acp-18-15003-2018.